ELSEVIER

Contents lists available at ScienceDirect

# **Chemical Physics Impact**

journal homepage: www.sciencedirect.com/journal/chemical-physics-impact



# Full Length Article

# Quantum computational, molecular structure, experimental spectra, and molecular docking studies on (*S*)-3-benzyl-5-(phenylselanyl)-6-(p-tolyl)-3,4-dihydropyran-2-one

S. Durgadevi <sup>a,b</sup>, C. Venkataraju <sup>a</sup>, Malik Nasibullah <sup>c</sup>, Mohd Asif <sup>c</sup>, Bhoopendra Tiwari <sup>d</sup>, A. Manikandan <sup>e,f</sup>, E. Geetha <sup>g</sup>, S. Muthu <sup>h,\*</sup>

#### ARTICLE INFO

# Keywords: DFT MEP NBO Hirshfeld Molecular docking

#### ABSTRACT

The published molecule (S)-3-Benzyl-5-(phenylselanyl)-6-(p-tolyl)-3,4-dihydropyran-2-one (3B6PL) was selected for the identification of anticancer properties, and the computational calculations were employed using density function theory (DFT) with the B3LYP/6-311++G (d,p) basis set to validate the proposed molecular structure features by the theoretical computational calculations, Herein, the FT-IR, UV-800, <sup>1</sup>H NMR, and <sup>13</sup>C NMR analytical techniques were used for the characterization of the selected molecule. In FT-IR, the characteristic frequencies of the molecule were compared using an appropriate scaling factor (0.961) for the potential energy distribution (PED) and simulated spectra of 3B6PL. Moreover, UV-800 and NMR spectral data were validated using the NBO that was demonstrated to the charge transfer in the molecules and exhibits a prominent secondorder perturbation energy, E(2) value is 309.85 kcal/mol. HOMO-LUMO, Molecular electrostatic potential (MEP) both find molecule's electrical properties, as well as its softness, hardness, and overall stability. To understand the reactive locations of the molecule, fukui functions have been employed. Moreover, the exceptional NLO (nonlinear optical) characteristics of the molecule were demonstrated, and intermolecular interactions were evaluated using a Hirshfeld surface as well. On the contrary, the druglikeness of the molecule was evaluated under Lipinski's rule of five and ADME/T studies. In-silico analysis and molecular docking were also demonstrated for the anticancer potential of the proposed molecule against the kinase insert domain receptors of VEGFR and showed binding affinities of -6.3 kcal/mol for the VEGFR-ligand complex as a preliminary investigation. Therefore, this compound could be used for in-vitro and in-vivo analyses to find out its cytotoxicity and could also be derivatized to enhance its potent anticancer properties.

#### 1. Introduction

Presently, disease of cancer is a common ailment among humans around the world. Nowadays, awareness as well as treatment related to cancer is needed, as is the synthesis of novel anticancer agents [1,2]. However, a published 3,5-dibenzyl-6-(p-tolyl)-3,4-dihydropyran-2-one

derivative was chosen for the biological evaluation [3]. The skeleton of the synthesized compound exhibited a drug-like molecule, so we selected to determine the anticancer properties using *in-silico* studies as well. Moreover, density function theory (DFT) was employed for validation of the characterization of synthesized compound. On the contrary, the FDA-approved drug 4-(3-(cyclopentyloxy)–4-methoxy

E-mail address: mutgee@gmail.com (S. Muthu).

<sup>&</sup>lt;sup>a</sup> PG and Research Department of Physics, Thiru.Vi.Ka Govt Arts College, Thiruvarur 610 003, Affiliated to Bharathidasan University, Tiruchirappali-24, Tamilnadu, India

b Department of Physics, Thalapathy K.Vinayakam Womens Arts and Science College, Tiruttani 631209, Tamilnadu, India

<sup>&</sup>lt;sup>c</sup> Research Lab-B043, Department of Chemistry, Integral University, Lucknow 226026, UP, India

d Department of Biological and Synthetic Chemisty, Centre of Biomedical Research, SGPGIMS-Campus, Raebareli Road, Lucknow 226014, U.P., India

<sup>&</sup>lt;sup>e</sup> Department of Chemistry, Karpagam Academy of Higher Education, Coimbatore - 641021, Tamil Nadu, India

f Centre for Material Chemistry, Karpagam Academy of Higher Education, Coimbatore - 641021, Tamil Nadu, India

g Department of Mathematics, Sri Chandrasekharendra Saraswathi viswa Mahavidyalaya, Enathur, Kanchipuram - 631561, India

<sup>&</sup>lt;sup>h</sup> Department of Physics, Arignar anna Govt. Arts College, Cheyyar 604 407, Tamilnadu, India

<sup>\*</sup> Corresponding author.

FDA approved drug Bevacizumab

Synthesized drug-like molecule

Fig. 1. Structure of bioactive molecules and their conformation.

phenyl)pyrrolidin-2-one (Bevacizumab) is known as a multipurpose drug for the treatment of many cancers [4]. Therefore, it was chosen as a standard ligand for the comparative studies with the synthesized molecule due to the conformation among the benzyl rings found in the same skeleton Fig 1.

The FDA has given the drug bevacizumab approval for the treatment of number of cancers, in spite of that non-small cell lung, colorectal, renal cell, cervical, ovarian, fallopian tube, peritoneal, glioblastoma multiforme and hepatocellular carcinomas [5]. The function of this drug is to inhibit the activity of the receptors located on the surface of endothelial cells, specially Flt-1 (VEGFR-1) and kinase insert domain receptor (VEGFR-2) binding to vascular endothelial growth factor (VEGF) through active sites found in the structure of the molecule and proteins. Hence, the demonstration of strong binding affinities among the residues of active sites of targeted proteins by the synthesized molecule as well as standard drugs has significant part in evaluation of the anticancer activities of synthesized compound as pre-screening [6]. In this research, we demonstrated the validation of the molecular structure by the DFT, when attempting to address the characteristics of enormous systems, the DFT technique effortlessly deal with many and difficult problems. Simulation results and experimental results can sometimes agree well. Because of its wide range application, it is significant in biological research. To anticipate the synthesis molecule's vibrational, electrical and structural characteristics with triple zeta basis set, a number of spectroscopic methods have been used, including FT-IR, UV, and NMR. Theoretical investigations of HOMO-LUMO, UV, MEP, NLO was performed for gas, DMSO, water, ethanol and acetone solvents. The NMR spectra and single crystal x-ray studies both supported the compound's structure. NBO is examined using the energy of inter-and intramolecular stabilization and not only that, we analyzed the drug-like properties with the help of computational chemistry like ADMET and molecular modeling as well.

#### 2. Materials and methods

# $2.1. \ \ \textit{To synthesis 3,5-dibenzyl-6-(p-tolyl)} - \textit{3,4-dihydropyran-2-one}$

Bhoopendra Tiwari et al. (2022), reported to the synthesis of 3,5-dibenzyl-6-(p-tolyl)-3,4-dihydropyran-2-one (3a) derivatives that was

published. We chose one molecule (**3 a**) for the biological demonstration as preliminary investigation like druglikeness, ADME/T, *in silico* analysis, on the basis of the skeleton core of the molecule. However, this molecule was synthesized using strategy as  $\alpha,\beta$ -unsaturated aldehydes **1a** (0.2 mmol) and selenyl vinyl ketones **2a** (0.1 mmol) were reacted in the presence of catalyst **A** (8 mg, 0.02 mmol) in 1.0 ml of room temperature in toluene. Argon was used to purge the reaction chamber before Cs<sub>2</sub>CO<sub>3</sub> (13 mg, 0.04 mmol) was introduced (Scheme 1). Following a 15-hour period of stirring the reaction mixture at ambient temperature, the solvents were removed using reduced-pressure evaporation. In order to make **3 a** in a 75 % yield with 99 % ee, the unprocessed material was purified through flash column chromatography employing silica gel and a mixture of ethyl acetate and hexane.

#### 2.2. Experimental details

The FT-IR Spectrometer of Agilent Cary 630 (Range: 4000–450 cm $^{-1}$ ), IIRC, Integral University, Lucknow was used to record the infrared spectra. DMSO-d $_6$  was used as the solvent and an Advance-400 MHz Brucker were generate  $^1\mathrm{H}$  NMR spectra. The internal standard was trimethylsilane, and the chemical shift were represented in ppm units. DMSO-d $_6$  was used to create the  $^{13}\mathrm{C}$  NMR spectra using a Brucker AVLL-100 MHz (Brucker, Switzerland). For UV spectra the wavelength recorded range 230–500 nm are determined using the kinetic Eppendorf Biospectrometer. For lattice parameters XRD -Bruker APEX-III CCD was utilized.

#### 3. Computational details

In computational methods, Gaussian 09 software [7] program package is used, Research has shown that the hybrid and correlation-functional method B3LYP can strike a favorable balance between the precision of vibrational spectra calculations for molecules of varying sizes (large and medium) and the computational effort required, utilizing DFT approach along with the 6-311++G (d,p) basis set [8]. Gaussian View [9] was utilized to perform geometric structure optimization and assign vibrational modes for the 3B6PL compound. The stationary points in DFT are all minima. By molecular structure optimization NBO interactions, HOMO-LUMO analysis, UV studies, NLO property, FUKUI functions and the frequencies of all possible vibrations with their PED values were obtained, The PED were carried out by VEDA [10]. By using frequency checkpoint were run the VEDA for Vibrational assignments and Multiwfn software [11] where we analysis the LOL and ELF. To acquire NMR chemical shift and identify the chemically important region, a GIAO technique was used in conjunction with experimental data. Using the crystal explorer [12] programme, the hirshfeld molecular surface and its 2D plots was created, the drug-likeness and ADME [13] features are attained by using online swiss ADME. Molecular docking was done by PyRx [14]. ChemDraw Professional version 15.1 and Chem3D version 15.1 [15] was used to design the two-dimensional and three-dimensional structures of the synthesized 3,5-dibenzyl-6-(p-tolyl)-3,4-dihydropyran-2-one, compound. Using the PDB ID: 1QTY, the 3D structure of VEGFR1 was downloaded from PDB (http://www.rcsb.org/) and represented by BIOVIA Discovery Studio Visualizer 2020 [16]. The structural alteration, geometrical

**Scheme 1.** Strategy for the formation of 3,5-dibenzyl-6-(p-tolyl)-3,4-dihydropyran-2-one.

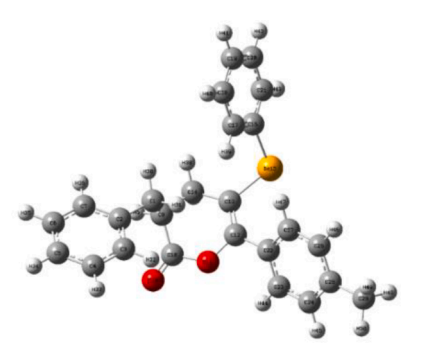


Fig. 2. Optimized structure of 3B6PL.

corrections and optimisation processes were carried out using Merck Molecular Force Field (MMFF94). Automatic hydrogen predictions are made by the web programme protoss for connection of protein-ligand complexes. (https://proteins.plus/). The graphical representations were made with Origin 6.0 programme [17,18].

#### 4. Results

#### 4.1. The geometrical analysis

The molecular geometry of (C25H22O2Se) compound for the gas phase 3B6PL was optimized at the DFT theory and the optimal structure as illustrated in Fig. 2 with gas ground state energy of -3518.1927 Hartree, it was discovered to exhibit the C1 point group symmetry [19]. The data from single crystal XRD and corresponding crystallographic information file (CIF) file of experimental values were used for comparison. The Cambridge crystallographic data centre (CCDC) has been given information on structure under the reference number CCDC 2,057, 769. It is discovered that 3B6PL has an orthorhombic crystal structure, with call dimensions of a = 9.3022 (5) Å, b = 9.9995 (5) Å, and c = 0.302221.2668 (12) Å at temperature 298 K. Lactones are the group of cyclic carboxylic ester. The oxygen atom double bonded to the carbon atom in part of completing the ring structure that carbon atom attached to another oxygen atom. No negative vibrational modes were produced by any of the optimized structure, demonstrating that they were all stationary points during the geometry optimization processes. [20] The maximum bond length is obtained for (Se15-C16) at 1.9411 Å and their experimental value 1.922 Å and (C13-Se15) at 1.9269 Å their respective experimental value found at 1.909 Å. The Typical length of C—C bond is 1.4264 Å, the angle of C—C-C bond ranges from  $130.37^{\circ}$  -  $108.96^{\circ}$ respectively. The molecule exhibit bond length of C8-C10, which is found to be 1.512 Å both theoretically and experimentally. The bond distance of C2-C3, C3-C4, C2-C7, C6-C7 and C16-C17 are found to be 1.391,1.395,1.39,1.39 and 1.397 Å (experimental) and slightly varied from theoretical values 1.398,1.399,1.393, 1.392 and 1.396 Å The data of the theoretical calculation for bond angle C-C-H group of C2-C3-H32,C4-C5-H34 and C25-C24-H45 are found experimentally at 119.5,120.2 and  $119.5^{\circ}$  and for theoretical outcome as 119.5,120.2 and 119.5° then C—C-C angle were C23-C22-C27 and C25-C26-C27 found at 118.3 and 121.3°(theoretical) with the experimental parameters of 118.3 and 121.3° [21]. Table (S1) demonstrates the high consistency between the DFT and XRD results when they are compared.

# 4.2. Vibrational assignments

By using vibrational spectroscopy, the molecule's functional group is identified. The compound 3B6PL has 50 atoms and 144 different vibrational modes. The calculated frequencies are reduced by 0.961 scale factor. In Table 1, the PED assignments were reported and the observed FT-IR are compared with theoretical values that have been calculated has seen in Fig. 3.

#### 4.2.1. C-H vibration

The stretching (Y) vibrations of C—H atom are visible at 3100–3000 cm<sup>-1</sup>. In 144–132 mode, the scaled wavenumbers 3034, 3039, 3044, 3054, 3065, and 3076 cm<sup>-1</sup> referred to Y(C—H) vibrations and have PED value of 90,92,99,94, and 93 %. The experimental value of 3031 cm<sup>-1</sup> is corresponds with the theoretical value with 90 % of PED. The wave numbers of C—H vibrations align with the anticipated range [22].

#### 4.2.2. C-C vibration

The frequencies of C—C stretching fall between 1650 and 1000  $\rm cm^{-1}$ . The frequency of phenyl rings are typically 1645, 1622, 1596, 686, 616  $\rm cm^{-1}$ . The calculated and scaled frequencies for the phenyl rings in title compound are 1596 and 1581  $\rm cm^{-1}$ , while the corresponding observed IR peaks are 1629 and 1574  $\rm cm^{-1}$ . The C—C bond in the 3B6PL has values ranging from 1661 to 616  $\rm cm^{-1}$ . [23] Theoretical C—C vibrational mode values are in close alignment with the results of experiments.

#### 4.2.3. C = O, C-O, and C-Se vibration

The regions attributed to C=O vibrations in IR spectroscopy are  $1780-1700~\rm cm^{-1}$ , in the current investigation, the mode of  $122~\rm with$  a wave number of  $1763~\rm cm^{-1}$  for C=O peak is determined theoretically and compared with experimental wavenumber of  $1766~\rm cm^{-1}$ , with  $89~\rm Wellow$  PED value [24]. When a molecule has a carbonyl group, the absorbance generated by C—O Stretching is frequently high. The C—O vibration's observed wavelength range is  $1095~\rm cm^{-1}$ , while perceived calculated values are  $1099~\rm cm^{-1}$ , and C—O bending vibration is  $616~\rm cm^{-1}$ , both sets of data are in agreement [25]. In IR Spectroscopy, the wavelength between  $600~\rm and$   $700~\rm cm^{-1}$  is generally absorbed by the selenium-carbon (Se-C) bond. The range  $650~\rm cm^{-1}$  this absorption is a calculated characteristics of the Se- C stretching vibration in the 3B6PL compound, and the experimental results are  $662~\rm cm^{-1}$  both values are resonated and lies in the range.

# 4.3. Frontier molecular orbital

It reveals compound's chemical reactivity and provides evidence of an eventual charge transfer with in molecules. In 3B6PL, high energy gap value indicates its classification as a hard molecule. Gas solvents has more energy gap value of 4.375 eV. It denotes hard nature when compared to other solvents such as (DMSO, Ethanol, Acetone, water) i.e. large HOMO-LUMO gap means less reactive [26]. The solvents effects are depicted in Fig. 4. The electron affinity and ionization potential are Associated directly to FMO values of donor and acceptor region. Compare to other solvents, gas shows minimum electron affinity value 1.451 eV it means the title compound has readily accept the electrons to create bond. Chemical stability may be good measure of chemical hardness. According to Table 2, the title molecule's chemical hardness was determined to be 2.187, which is a high value and suggested that the molecule is chemically stable. The title molecule, which has a low chemical softness of 0.229, also discovered to be theoretically non-harmful. The title molecule possess high molecular hardness with that of low softness values gives directly assess the electrophilicity index has explain the biological activity of title compound [27].

# 4.4. UV spectral analysis

TD-DFT was employed to perform UV- Vis characterization of the 3B6PL compound in some kinds of non-polar and polar solvents and the absorption maxima for molecules lower-energy singlet states were calculated using the B3LYP method [28]. Fig. 5 displays the experimental findings together with a comparison of the theoretical spectrum. The calculated values of the oscillatory strength, transition coefficient, absorption wavelength, and assignments are compared with experimental values. The estimated maximum absorption wavelength in gas phase, Acetone, DMSO, ethanol and water (338.17 nm, 341.42 nm,

Table 1
Calculated and observed Vibrational frequency with assignments for 3B6PL

No. of MODES	Experimental frequency	Theoritical	frequency	IR INTENS	SITY	RAMAN A	CTIVITY	PED % <sup>c</sup>	
	IR	Unscaled	Scaled d	Relative	Absolute <sup>a</sup>	Relative	Absolute <sup>b</sup>		
.44	_	3201	3076	4.212	0.94	103.6	13.41	Y(CH)(93)	
43	_	3197	3073	4.691	1.05	68.98	8.93	Υ(CH)(93)	
42	_	3192	3068	14.58	3.27	388.2	50.25	Υ(CH)(94)	
41	_	3189	3065	16.96	3.80	332.9	43.09	Y(CH)(91)	
40	_	3185	3061	17.91	4.02	20.77	2.69	Y(CH)(97)	
39	_	3178	3054	8.047	1.80	119.6	15.48	Υ(CH)(92)	
38	_	3177	3053	26.12	5.86	54.40	7.04	Υ(CH)(82)	
37	_	3168	3044	1.468	0.33	113.6	14.70	Y(CH)(96)	
.36	_	3167	3043	6.452	1.45	105.7	13.68	Y(CH)(86)	
.35	_	3162	3039	1.450	0.33	16.27	2.11	Υ(CH)(90),	
34	_	3161	3038	19.69	4.42	124.2	16.08	Υ(CH)(86),	
.33	_	3160	3037	12.07	2.71	100.7	13.04	Υ(CH)(89),	
.32	3031	3157	3034	5.068	1.14	51.70	6.69	Y(CH)(88),	
.31	_	3150	3027	8.744	1.96	40.33	5.22	Υ(CH)(92),	
.30	_	3102	2981	14.48	3.25	73.24	9.48	Y(CH)(96),	
29	_	3091	2970	20.13	4.51	29.05	3.76	Y(CH)(92),	
28	_	3076	2956	8.966	2.01	91.32	11.82	Y(CH)(91),	
27	_	3075	2955	10.50	2.35	115.7	14.97	Υ(CH)(91),	
26	_	3063	2944	6.551	1.47	58.60	7.58	Υ(CH)(92),	
25	2927	3035	2917	20.35	4.56	105.1	13.61	Υ(CH)(82),	
24	_	3021	2903	33.98	7.62	432.9	56.03	Υ(CH)(98),	
23		3010	2893	18.71	4.20	172.9	22.38	Υ(CH)(92),	
22	1766	1835	1763	446.0	100.0	36.37	4.71	Y(OC)(90),	
.21	1629	1661	1596	68.67	15.40	772.6	100.0	Y(CC)(78),	
.20		1651	1587	14.67	3.29	286.6	37.10	$\Upsilon(CC)(62),\beta(HCC)(16),\beta(CCC)(10),$	
19	1574	1645	1581	5.979	1.34	52.29	6.77	Υ(CC)(58),β(HCC)(24),	
18	_	1624	1561	1.152	0.26	10.18	1.32	Υ(CC)(52),β(HCC)(10),	
17	_	1618	1555	35.35	7.93	88.97	11.52	Υ(CC)(63),β(HCC)(17),	
.16	_	1612	1549	0.649	0.15	23.97	3.10	$\Upsilon$ (CC)(51), $\beta$ (CCC)(10),	
15	1508	1602	1539	0.830	0.19	12.94	1.67	Υ(CC)(59),β(HCC)(13),	
14	1496	1541	1481	22.19	4.98	14.78	1.91	β(HCC)(60),β(CCC)(10),	
.13	1473	1527	1468	11.21	2.51	0.70	0.09	β(HCC)(59),β(CCC)(18),	
12	_	1505	1446	30.15	6.76	1.32	0.17	β(HCC)(66),β(CCC)(17),	
111	_	1494	1435	2.920	0.65	7.15	0.92	β(HCH)(80),	
10	1434	1492	1434	9.886	2.22	8.45	1.09	β(HCH)(68),Ţ(HCCC)(20),	
109	_	1490	1432	6.945	1.56	19.23	2.49	β(HCH)(77),Ţ(HCCC)(21),	
108	_	1484	1426	3.177	0.71	3.42	0.44	β(HCC)(44),	
.07	_	1478	1421	3.124	0.70	33.28	4.31	β(HCH)(81),	
106	_	1467	1410	7.736	1.73	1.71	0.22	Υ(CC)(18),β(HCC)(56),	
.05	_	1434	1378	1.751	0.39	2.24	0.29	Υ(CC)(36),β(HCC)(31),	
104	_	1414	1359	0.637	0.14	37.28	4.83	β(HCH)(95),	
.03	_	1382	1328	35.70	8.01	15.80	2.04	β(HCC)(18),Ţ(HCCC)(22),	
.02	_	1368	1314	2.821	0.63	9.23	1.19	β(HCC)(44),T(HCCC)(16),T(HCCO)(14),	
.01	_	1352	1299	0.589	0.13	11.18	1.45	Υ(CC)(15),β(HCC)(27),Ţ(HCCC)(12),Ţ(HCCO)(1	
.00	_	1347	1295	1.253	0.28	5.12	0.66	Υ(CC)(11),β(HCC)(75),	
19	_	1342	1290	3.978	0.89	10.89	1.41	β(HCC)(30),Ţ(HCCC)(13),	
18	_	1339	1287	2.568	0.58	6.90	0.89	β(HCC)(50),	
7	_	1335	1283	0.202	0.05	2.29	0.30	Υ(CC)(57),Ţ(HCCO)(11),	
16	_	1322	1271	1.107	0.25	22.06	2.86	Y(CC)(66),	
5	_	1312	1261	0.961	0.22	7.89	1.02	Υ(CC)(68),β(HCC)(11),	
94	_	1286	1236	43.10	9.67	104.6	13.54	Υ(CC)(11),β(HCC)(33),Ţ(HCCO)(10),	
93	1209	1264	1214	3.307	0.74	75.87	9.82	Υ(CC)(19),β(HCC)(11),	
2	_	1233	1185	8.080	1.81	3.45	0.45	β(HCC)(39),Ţ(HCCC)(17),	
01	_	1232	1184	0.235	0.05	47.50	6.15	Υ(CC)(66),β(HCC)(13),	
90	_	1227	1179	4.046	0.91	25.58	3.31	Υ(CC)(36),β(HCC)(16),β(CCC)(11),	
89	_	1212	1165	7.436	1.67	19.44	2.52	Υ(CC)(15),β(HCC)(58),	
38	_	1204	1157	6.466	1.45	2.05	0.27	Y(CC)(15),T(HCCC)(10),	
37	_	1204	1157	46.12	10.34	29.17	3.78	β(HCC)(83),	
86	1155	1202	1156	11.47	2.57	15.79	2.04	Υ(CC)(17),β(HCC)(59),	
85	1142	1182	1136	0.026	0.01	3.77	0.49	Υ(CC)(14),β(HCC)(65),	
4	_	1182	1136	1.549	0.35	4.52	0.59	β(HCC)(64),	
3	_	1153	1108	33.84	7.59	11.62	1.50	Υ(OC)(14),β(HCC)(24),	
2	1095	1143	1099	33.87	7.59	1.62	0.21	Υ(CC)(22),β(HCC)(46),	
51	-	1107	1063	117.2	26.28	5.57	0.72	Υ(CC)(43),β(HCC)(21),	
30	_	1097	1054	26.30	5.90	1.71	0.22	Υ(CC)(34),β(HCC)(37),	
79	_	1096	1054	245.0	54.95	10.49	1.36	Υ(CC)(22),Υ(OC)(16),	
'8	- 1026	1090	1034	3.284	0.74	14.84	1.92	β(CCC)(10),β(HCC)(27),β(CCC)(33),	
o 7	1019	1060	1039	14.35	3.22	0.40	0.05	β(HCH)(15),T(HCCC)(61),	
	1019	1053	1018	56.25	3.22 12.62	3.05	0.05	$\Upsilon(CC)(16),$	
'6 '5									
	_	1050	1009	2.267	0.51	18.41	2.38	Υ(CC)(31),β(HCC)(19),β(CCC)(22), Υ(CC)(12),β(CCC)(18)	
'4 '2	- 007	1042	1001	4.836	1.08	5.83	0.76	Υ(CC)(12),β(OCO)(18), Υ(CC)(14),β(CCC)(15)	
73	997	1039	998	15.31	3.43	42.12	5.45	Υ(CC)(44),β(CCC)(15),	
72	-	1032	992	23.13	5.19	7.73	1.00	β(CCSe)(41),	

(continued on next page)

Table 1 (continued)

No. of MODES	Experimental frequency	Theoritical	frequency	IR INTENS	SITY	RAMAN A	CTIVITY	PED % <sup>c</sup>
	IR	Unscaled	Scaled d	Relative	Absolute <sup>a</sup>	Relative	Absolute <sup>b</sup>	
71	_	1018	978	1.098	0.25	42.45	5.49	Υ(CC)(45),
70	_	1013	974	2.129	0.48	77.30	10.01	Υ(CC)(38),β(CCC)(49),
59	_	1008	968	8.364	1.88	0.75	0.10	β(HCH)(19),Ţ(HCCC)(56),
58	-	1002	963	0.577	0.13	0.43	0.06	T(HCCC)(76),T(CCCC)(13),
57	-	998.1	959	3.956	0.89	0.71	0.09	T(HCCC)(75),T(CCCC)(10),
56	-	993.3	955	34.72	7.79	12.82	1.66	β(COC)(10),β(OCC)(14),β(CCO)(16),
55	-	989.6	951	115.4	25.87	4.35	0.56	Y(OC)(13),
64	-	984.9	946	0.851	0.19	0.19	0.02	β(HCC)(64),Ţ(HCCC)(89),
63	-	984.3	946	2.618	0.59	3.49	0.45	T(HCCC)(86)
62	-	979.1	941	0.703	0.16	0.09	0.01	T(HCCC)(74),T(CCCC)(21)
51	917	967.1 932.0	929 896	1.184	0.27 1.42	0.21	0.03	T(HCCC)(69),T(CCCC)(16)
50 59	_	932.0 919.6	896 884	6.310 12.40	2.78	1.04 0.88	0.14 0.11	T(HCCC)(36), T(HCCC)(67),
58	_	918.5	883	5.647	1.27	1.58	0.11	((11000)(07),
57 57	_	876.6	842	7.366	1.65	12.21	1.58	$\Upsilon(CC)(22),\omega(CCSeC)(18),$
56	823	853.8	820	0.340	0.08	0.89	0.12	T(HCCC)(96),
55	_	851.5	818	0.208	0.05	0.25	0.03	T(HCCC)(96),
54	_	849.3	816	7.934	1.78	6.18	0.80	T(HCCC)(66),
53	_	842.8	810	8.820	1.98	2.22	0.29	Y(CC)(11),T(HCCC)(68),
52	_	833.9	801	18.65	4.18	3.93	0.51	T(HCCC)(40),
51	789	816.2	784	5.080	1.14	20.23	2.62	Υ(CC)(30),β(CCC)(16),
50	-	791.7	761	8.060	1.81	24.71	3.20	Y(OC)(37),
49	737	756.3	727	21.82	4.89	7.16	0.93	Ţ(HCCC)(42),
48	719	748.6	719	49.02	10.99	0.51	0.07	T(HCCC)(76),T(CCCC)(11),
47	-	741.9	713	3.725	0.84	1.35	0.18	ω(OCOC)(38),
46	-	734.0	705	5.753	1.29	2.46	0.32	T(HCCC)(19),
45	690	709.8	682	37.67	8.45	0.15	0.02	T(HCCC)(36),T(CCCC)(42),
14	-	706.5	679	23.14	5.19	0.53	0.07	Ţ(HCCC)(29),Ţ(CCCC)(41),ω(CCCC)(19),
43	662	676.6	650	7.822	1.75	5.62	0.73	Υ(SeC)(17),β(CCC)(62),
42	-	670.2	644	3.196	0.72	5.61	0.73	β(CCC)(29),ω(CCOC)(21),
41	622	660.1	634	2.720	0.61	4.53	0.59	0(000)(90) (0000)(10)
40	-	641.0	616	3.115	0.70	4.53	0.59	β(CCC)(39),ω(CCOC)(18),
39 38	611	635.8 629.6	611 605	0.227 0.147	0.05 0.03	4.27 4.19	0.55 0.54	β(CCC)(92),
37	-	616.3	592	14.78	3.32	3.28	0.42	β(CCC)(78), Υ(SeC)(11),β(CCSe)(28),
36	_	601.7	578	3.189	0.72	3.00	0.42	β(CCC)(31),
35		555.7	534	9.900	2.22	2.96	0.38	β(CCC)(11),β(CCO)(10),
34	_	528.3	508	14.42	3.23	1.55	0.20	β(COC)(15),β(CCO)(12),
33	_	507.6	488	4.412	0.99	3.70	0.48	T(CCCC)(34),ω(CCCC)(11),
32	_	485.6	467	6.072	1.36	3.59	0.46	β(CCSe)(10),T(CCCC)(17),
31	_	472.2	454	8.503	1.91	0.80	0.10	T(CCCC)(53),
30	_	415.3	399	0.045	0.01	6.48	0.84	T(CCCC)(70),
29	_	413.5	397	0.021	0.00	0.04	0.00	T(HCCC)(24),T(CCCC)(72),
28	_	410.7	395	0.289	0.06	0.17	0.02	Ţ(HCCC)(19),Ţ(CCCC)(66),
27	-	396.8	381	3.765	0.84	0.64	0.08	β(CCC)(37),
26	-	378.1	363	5.868	1.32	1.18	0.15	ω(OCOC)(13),
25	-	356.3	342	3.119	0.70	0.94	0.12	β(CCC)(17),
24	-	349.3	336	0.327	0.07	0.96	0.12	β(CCC)(40),
23	_	332	319	1.314	0.29	0.43	0.06	β(CCC)(32),
22	-	302.6	291	1.369	0.31	1.99	0.26	β(CCC)(12),Ţ(CCCC)(10),
21	-	300.2	288	0.562	0.13	1.49	0.19	$\Upsilon(SeC)(44),\beta(CCC)(10),$
20	-	290.8	279	1.079	0.24	2.99	0.39	T(OCCSe)(10),
19	-	254.9	245	0.145	0.03	4.78	0.62	β(SeCC)(20),ω(CCSeC)(11),
18	-	239.4	230	0.573	0.13	5.38	0.70	β(SeCC)(33),
17	-	219.6	211	0.817	0.18	3.96	0.51	Y(SeC)(23),T(OCCSe)(14),
16	-	194.9	187	0.539	0.12	2.44	0.32	β(CCC)(15),Ţ(CCCC)(10), Τ(CCCC)(11) α(CCCC)(41)
15 14	-	175.9 153.2	169 147	1.266 1.509	0.28 0.34	2.83 1.75	0.37 0.23	Ţ(CCCC)(11),ω(CCCC)(41),
13	-	140.1	135	1.543	0.34	1.75	0.23	β(CCSe)(16),β(CCC)(11), T(CCCC)(18),ω(OCOC)(10),
12	_	107.2	103	0.409	0.09	3.12	0.40	T(CCCO)(22),
12	_	89.29	86	1.126	0.09	2.96	0.40	β(CCC)(13),β(CSeC)(10),Ţ(CCCC)(13),Ţ(CCOC)(13
10	_	71.35	69	0.646	0.23	1.19	0.15	β(CCO)(10),β(CSeC)(16),
9	_	64.91	62	1.175	0.14	1.09	0.13	β(CCC)(11),Ţ(CCCC)(11),Ţ(CCCO)(15),Ţ(CCCC)(1
8	_	52.04	50	0.874	0.20	2.11	0.14	T(CCCC)(49),ω(CCOC)(11),
7	_	49.98	48	0.276	0.06	0.80	0.10	T(HCCC)(97),
6	_	41.95	40	0.323	0.07	7.50	0.10	T(CCCC)(72),
5	_	38.53	37	0.072	0.02	6.24	0.81	T(CCCC)(59),
4	_	28.47	27	0.083	0.02	3.74	0.48	T(CCCC)(80),
3	_	25.89	25	0.046	0.01	2.52	0.33	β(CSeC)(16),Ţ(CCSeC)(14),Ţ(OCCSe)(12),
2	_	15.87	15	0.137	0.03	2.54	0.33	T(CCSeC)(15),T(CCCC)(47),T(CCCO)(12),
1		14.29	14	0.155	0.03	5.02	0.65	T(CCSeC)(51),T(CCCC)(12),

 $<sup>^</sup>a$  relative absorption intensities normalized with highest peak absorption equal to 100.  $^b$  relative raman intensities normalized to 100.  $^c$  Y-stretching,  $\beta$ -bending,  $\uparrow$ -torsion,  $\omega$ - out plane bending.  $^d$  Scale factor: 0.961.

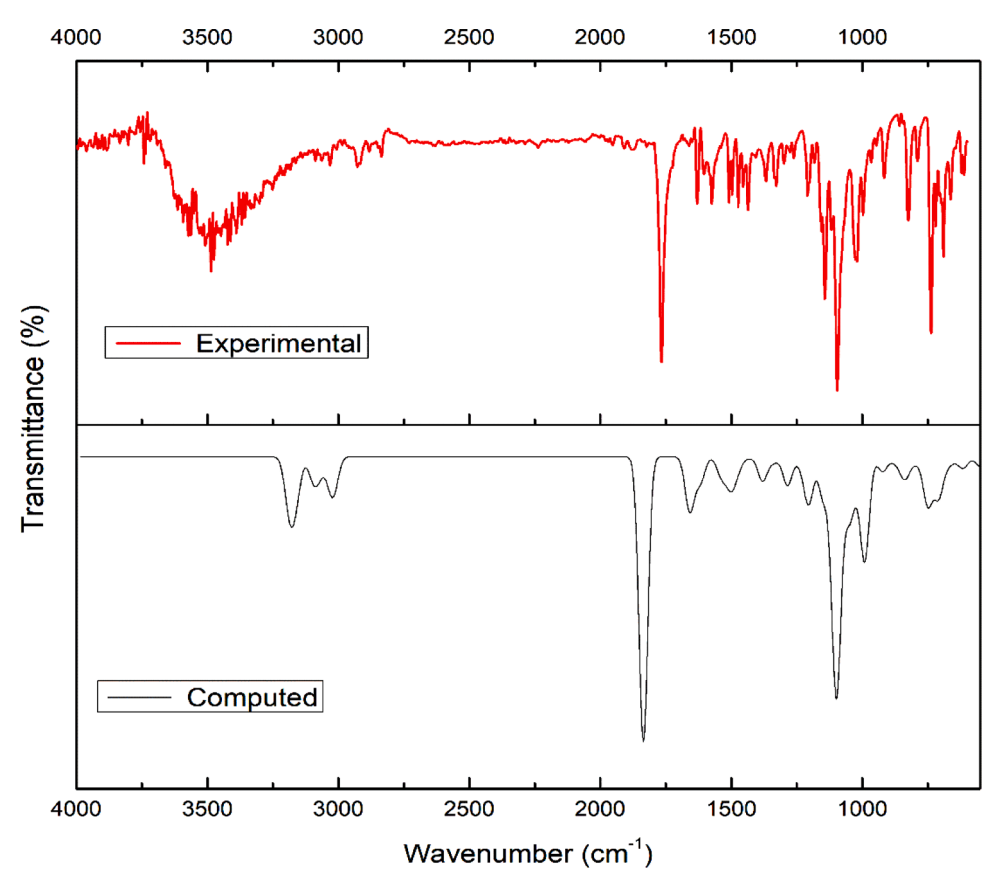


Fig. 3. FT-IR Spectra of 3B6PL.

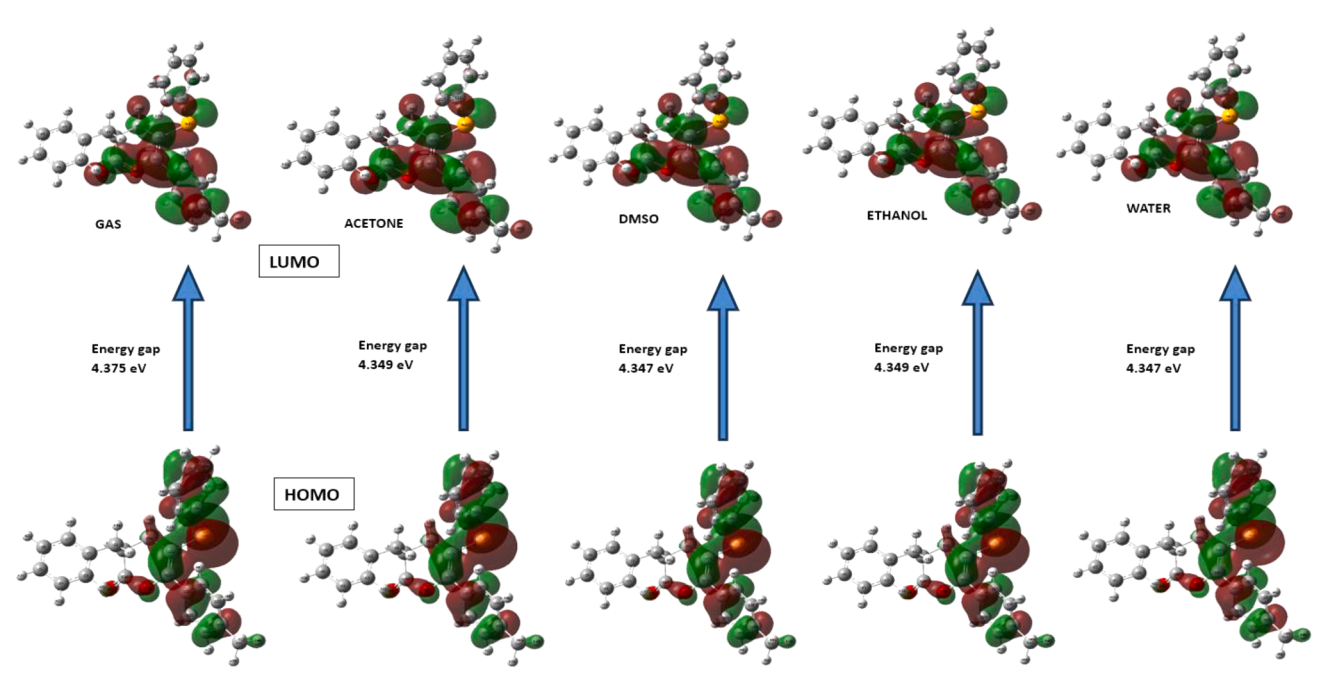


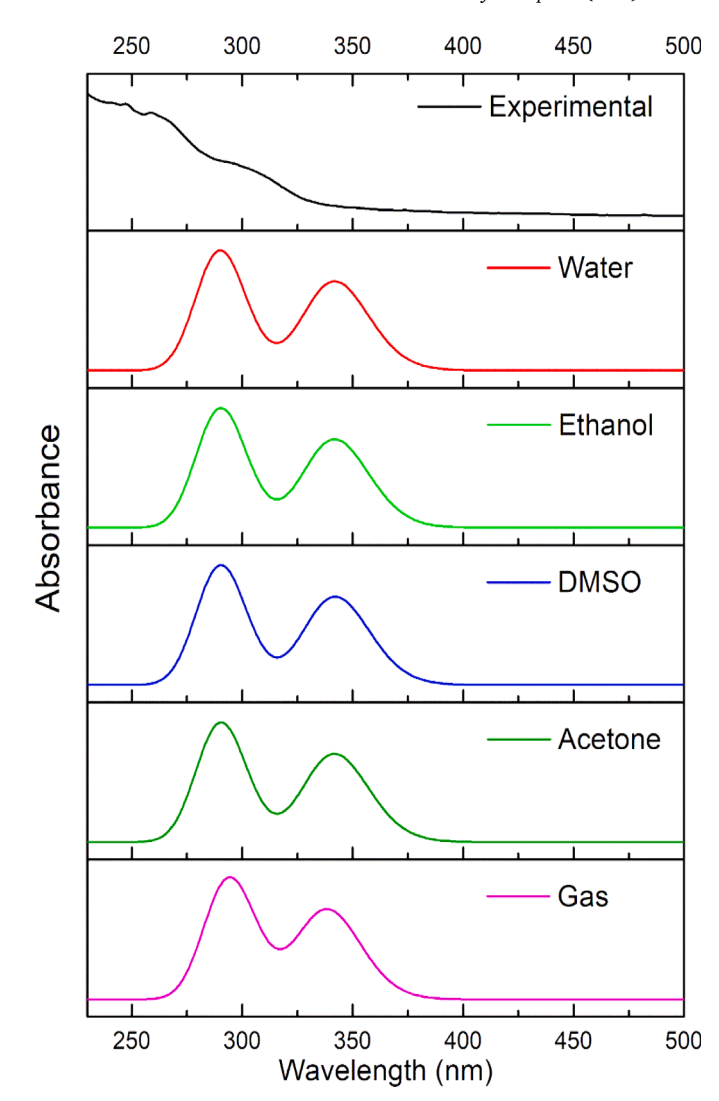
Fig. 4. HOMO-LUMO plots of various solvent effects for 3B6PL.

341.74 nm, 341.46 nm, and 341.48 nm) the solvents moreover in same wavelength, with corresponding energy values are E=3.666eV, 3.631eV, 3.631eV and 3.630eV accordingly. The simulated energy gap values are represented in Table 3. The observed absorption wavelength in solid phase was 247 nm, it means the shift towards Red,

with corresponding high Band gap value are 5.02 eV, when compare to theoretical. Table (3) lists the solvents with the highest HOMO-LUMO contribution (96 %). From the solid phase depicts the smaller value of wavelength at 247 nm, it shows better electronic properties [29].

Calculated energy values of 3B6PL.

	номо (еv)	LUMO (eV)	Ionization potential	Electron affinity	Energy gap (eV)	Electronegativity	Chemical potential	Chemical hardness	Chemical softness	Electrophilicity index	electronic charge	electron donating capability (w-)	electron accepting capability $(w+)$
Gas	-5.83	-1.45	5.83	1.45	4.38	3.64	-3.64	2.187	0.23	3.03	1.66	5.12	1.48
water	-5.89	-1.54	5.89	1.54	4.35	3.71	-3.71	2.173	0.23	3.17	1.71	5.3	1.59
ethanol	-5.88	-1.53	5.88	1.53	4.35	3.71	-3.71	2.174	0.23	3.16	1.71	5.29	1.58
DMSO	-5.89	-1.54	5.89	1.54	4.35	3.71	-3.71	2.174	0.23	3.17	1.71	5.3	1.59
Acetone	-5.88	-1.53	5.88	1.53	4.35	3.71	-3.71	2.174	0.23	3.16	1.7	5.28	1.58



 $\begin{tabular}{lll} {\bf Fig.} & {\bf 5.} & {\bf Simulated} & {\bf and} & {\bf experimental} & {\bf UV-Vis} & {\bf spectra} & {\bf of} & {\bf 3B6PL} & {\bf with} \\ {\bf different solvents.} & & & & \\ \end{tabular}$ 

# 4.5. MEP

The relationship between the distribution of nucleophilic and electrophilic charges in three-dimensional space around molecules can be understood with the help of MEP surface charts, which provide important visual indicators. It aids in determining the 3B6PL compound's electrostatic potential, size, shape, and reactivity. By using color grading, MEP values are displayed. The generated MEP surface map, which was created after analysis of the data, revealed that the compound's negative area are located near the oxygen atom, which represent strong negative electrostatic potential and indicates an electrophilic attack [30]. Whereas blue indicates the maximum positive electrostatic potential around the hydrogen atoms, which indicates a powerful attraction known as a nucleophilic attack. The investigated molecule's potential range include  $-5.557 \, e^{-2}$  to  $5.557 \, e^{-2}$  (gas),  $-6.718 \, e^{-2}$  to  $6.718 \, e^{-2}$  (acetone),  $-6.787e^{-2}$  to  $6.787e^{-2}$  (DMSO),  $-6.739e^{-2}$  to  $6.739 \, e^{-2}$  (ethanol),  $-6.809 \, e^{-2}$  to  $6.809 \, e^{-2}$  (water). As gas and solvation's are moreover with the same potential, that atoms are represented. The color grading in decreasing sequence, as seen in Fig. 6, is blue > green> red. MEP surface with electron deficient sites is blue, while those with neutral areas are a light green shade. Green signifies zero electrostatic potential, whereas a small amount of yellow colour around the carbon of phenylselenyl and benzyl rings suggests low

**Table 3**Experimental and theoretical values of electronic properties for 3B6PLcompound with various solvents.

Experimental		Theoretical	Theoretical								
Wavelength (nm)	Band gap(eV)	Solvents	Energy (eV)	Wavelength (nm)	Band gap(eV)	Osc. Strength (a.u)	Major contribs <sup>a</sup>				
247	5.02	Gas	3.6663	338.17	3.666	0.0958	H->L(95 %)				
		Acetone	3.6314	341.42	3.631	0.1219	H -> L(96 %)				
		DMSO	3.6280	341.74	3.628	0.1254	H -> L(96 %)				
		Ethanol	3.6309	341.46	3.631	0.1219	H>L(96 %)				
		Water	3.6307	341.48	3.631	0.1196	H ->L (96 %)				

<sup>&</sup>lt;sup>a</sup> -H-Homo, L- Lumo.

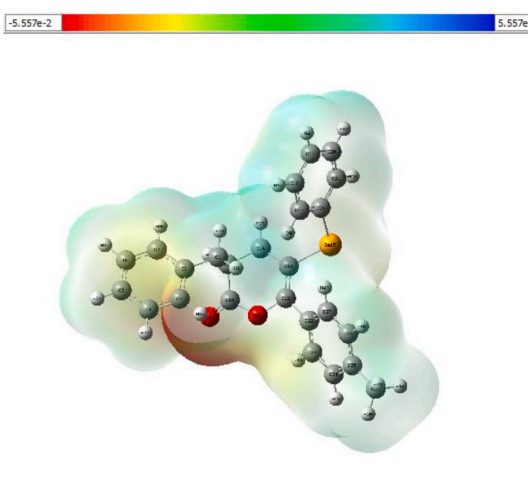


Fig. 6. MEP map of 3B6PL compound.

electrostatic potential [31]. The more negatively charged red surface region is more suited to interact with atoms that lack electrons. The fact that 3B6PL possesses a negative potential at the location of the oxygen (O29) atom indicates that the compound may have biological action.

#### 4.6. Lol and ELF

The ELF and LOL colour-filled maps produced by the multiwfn 3.8 program describe the interaction due to covalent bonding, which demonstrates molecular orbital delocalization. The ELF map in the current investigation has a scale spectrum that spans from 0.000 to 1.000 as represented in Fig. 7. The presence of carbon atoms on a blue surface with a lesser than 0.500 range indicates that the electron is delocalized and scale values larger than 0.500 reveal a strong ELF region [32], which indicates that the H-atom in the red surface area is highly localized. The LOL map has a region of 0.0 to 0.8 bohr, and LOL reaches its highest value with a value of more than 0.5, the white area in the middle of the hydrogen atom in (H30,H35) indicates an electron density that is more than 0.8 it is more than the highest limit of the colour scale.

### 4.7. Hirshfeld surface analysis

Investigations of interaction within the molecular structure is done using hirshfeld surface analysis. The 3B6PL compound uses CIF as input file. In 3B6PL, surface analysis and 2D finger prints were created. The title compound in 3D with several parameters, including dnorm (-0.1607-1.2617), shape index (-1.0000-1.0000) and curvedness (-4.0000-0.4000) were shown in the Fig. 8a. it is explicable by the colour scheme, red areas denote near proximity to neighbor molecule, blue spots longer proximity, and white spots proximity around

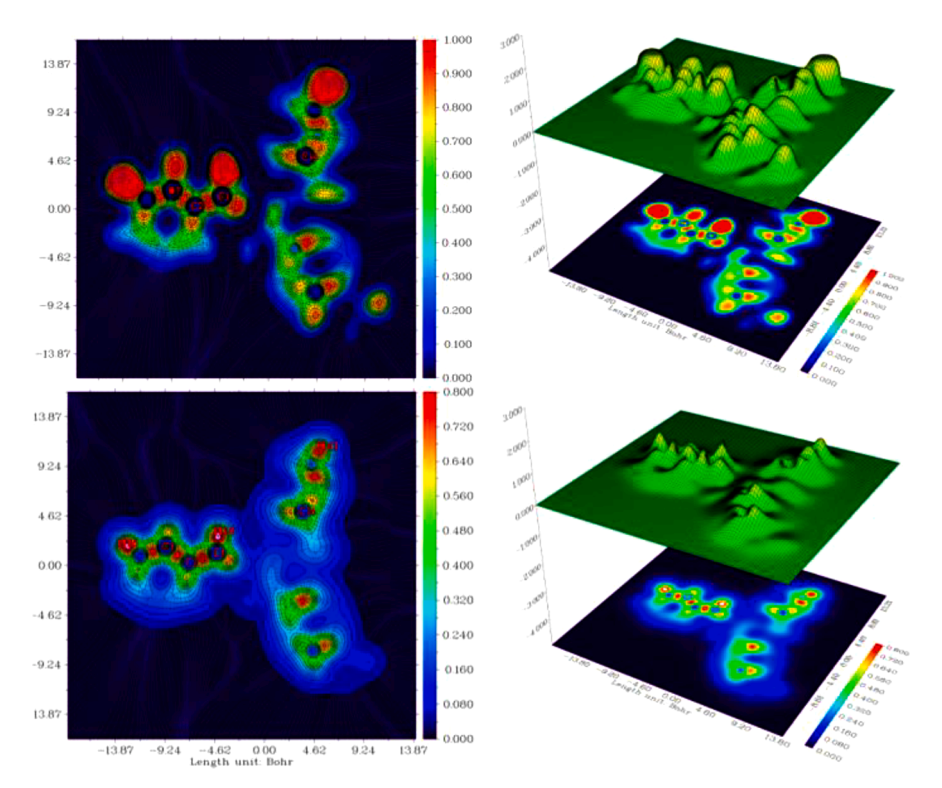


Fig. 7. ELF and LOL colored diagram and contour maps.

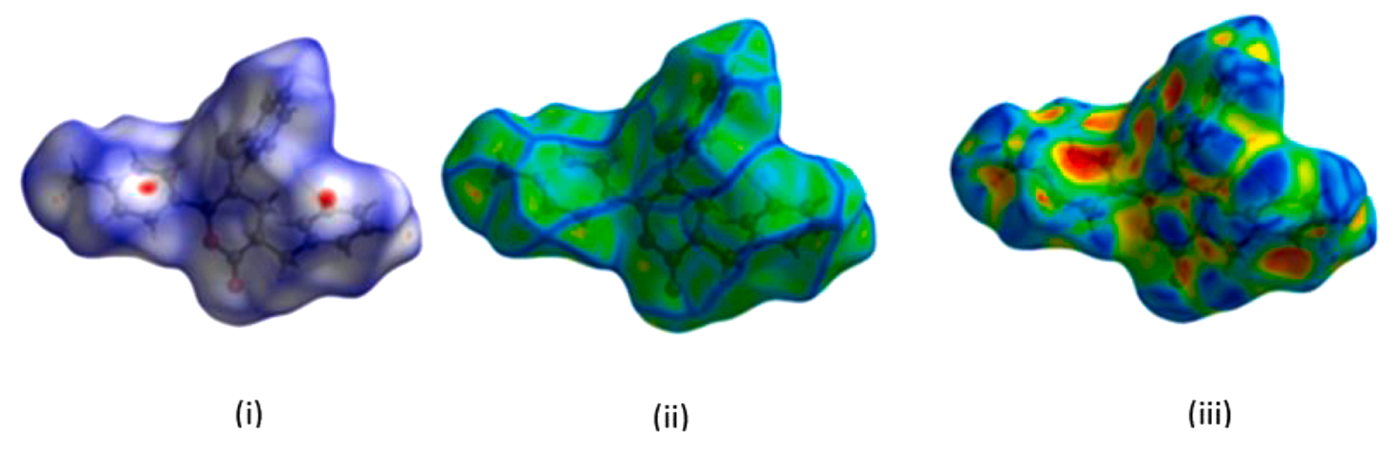
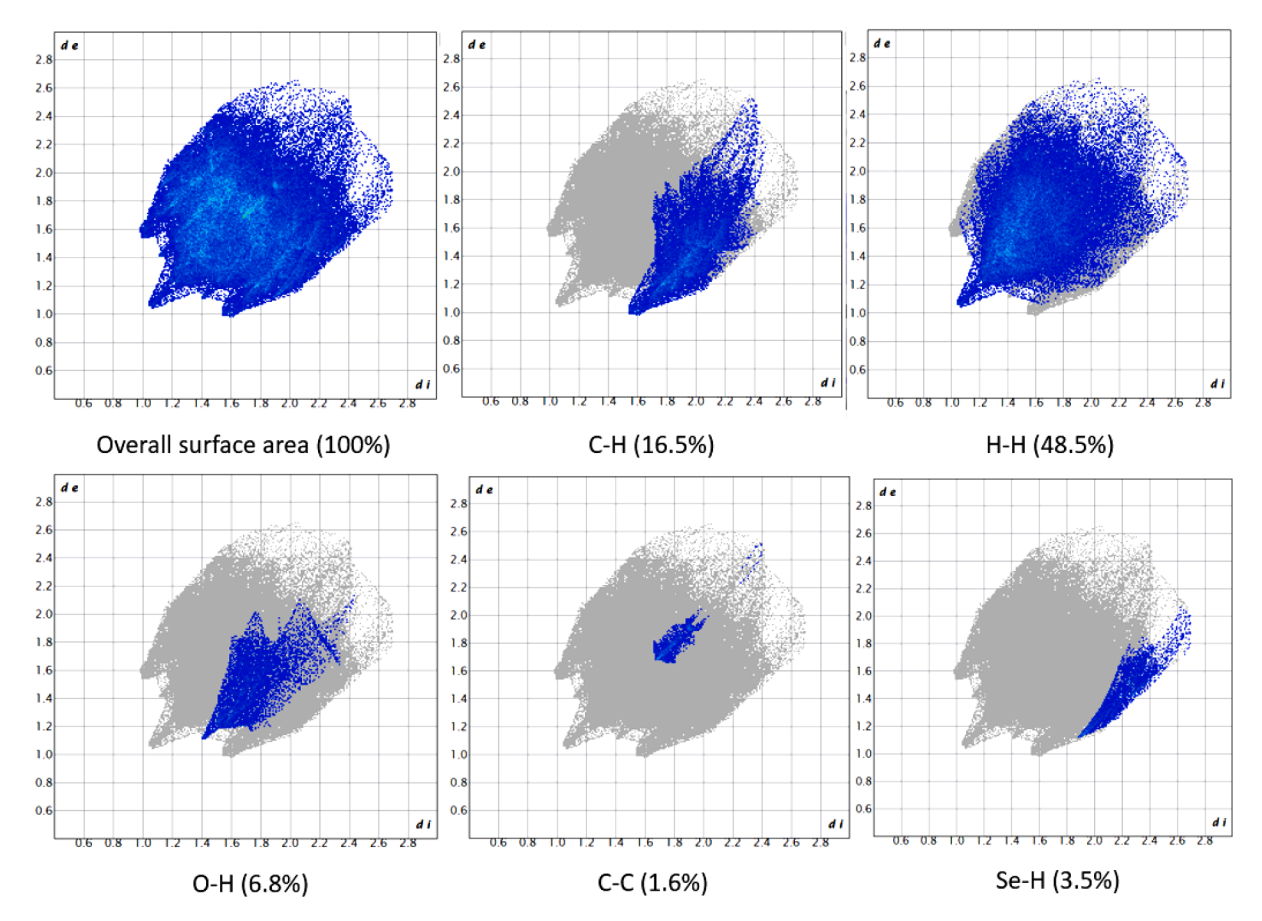


Fig. 8. a) Hirshfeld surface (i)dnorm, (ii)curvedness, (iii) shapeindex.



 $\textbf{Fig. 8.} \ \ \textbf{b)} \ \ \textbf{Fingerprint plots view of total surface of 3B6PL compound with individual contribution.}$ 

vanderwalls separation [33,34]. Over all molecules in a full fingerprint interaction, the interior and exterior intermolecular contacts have contributed. In two-dimensional finger print plots on the hirshfeld surface and their percentage contributions are displayed in Fig. 8b. The significant interaction determined with H—H(48.5 %),C—H(16.5 %), O—H(6.8 %),Se-H(3.5 %) surface with neighboring molecules.

# 4.8. NBO analysis

The NBO analysis utilized to identified the orbital bonding's maximum electron density, transferring of charges, interactions of donor and acceptors of 3B6PL molecule. To determine intra- and intermolecular bonding's as well as donor and acceptors stabilization energies E(2),

in NBO by applying second order perturbation theory. The intense interaction it indicates across accepting and donating electrons shows large stabilization energy. In the study it shows the transportation of charges from antibonding  $\pi^*$  (C16-C21) with occupancy of 0.3854 to  $\pi^*$  (C19-C20) with the occupancy of 0.3356 involving highest stabilization energy of 309.85 kcal/mol. The lone pair electron donor LP(2)-O29 has been shown to interact strongly with antibonding acceptor  $\sigma^*$  (C10-O11) is reason for strong electron delocalization it cause the next maximum E2 value of 36.65 kcal/mol and this lone pair with antibonding  $\sigma^*$  (C8-C10) having the energy value 17.13 kcal/mol. [35] The hyperconjugative interaction between LP(O) atom and the  $\pi^*$  orbitals LP (2)-O11  $\rightarrow$   $\pi^*$  (C10-O29) and  $\pi^*$  (C12-C13) has the next high E2 value of 33.04 and 25.28 kcal/mol. The delocalization of  $\pi$  electrons from

**Table 4**The calculated NLO properties of 3B6PL.

NLO properties	GAS	ACETONE	DMSO	ETHANOL	WATER	NLO properties	GAS	ACETONE	DMSO	ETHANOL	WATER
Dipole moment	μ (debye)					Hyperpolarizabi	lityβ (x10 <sup>-30</sup> e	e.s.u)			
μx	0.6890	0.8962	0.9045	0.8988	0.9072	βxxx	-39.5949	-75.8228	-68.7023	-73.8373	-65.9788
μy	0.9679	1.4485	1.4819	1.4586	1.4929	βχχ	173.6488	269.022	269.66	269.3099	269.6722
μz	0.8459	1.1085	1.1265	1.1139	1.1325	βхуу	-90.9188	-354.438	-377.308	-361.294	-385.035
μ(D)	1.4585	2.0323	2.0696	2.0436	2.0819	βууу	247.7276	216.9974	196.4095	211.0237	189.042
Polarizabilityα (	$(x10^{-23}e.s.u)$					βzxx	-35.9561	-86.0071	-87.1773	-86.4065	-87.4694
αxx	350.0047	449.3775	455.2962	451.1786	457.2401	βxyz	65.80709	155.7779	163.6877	158.1318	166.3998
αχγ	-4.5601	-1.9923	-1.7918	-1.9311	-1.7264	βzyy	192.1149	341.9156	349.088	344.1388	351.3563
αγγ	397.6971	536.9175	545.2331	539.4494	547.9609	βxzz	22.21748	22.54518	23.42244	22.79982	23.73473
αxz	8.9833	11.7009	11.8510	11.7468	11.8998	βyzz	237.5173	524.2406	545.9551	530.8168	553.145
αyz	0.3692	0.9524	0.7961	0.9095	0.7348	βzzz	-23.0456	-141.75	-163.189	-147.977	-170.862
αzz	256.2608	368.2379	376.9380	370.8570	379.8544	βtot (e.s.u)	$5.88e^{-30}$	$9.46e^{-30}$	$9.51e^{-30}$	$9.48e^{-30}$	$9.52e^{-30}$
α (e.s.u)	$4.96e^{-23}$	$6.69e^{-23}$	$6.80e^{-23}$	$6.73e^{-23}$	$6.84e^{-23}$						
$\Delta\alpha$ (e.s.u)	$9.17e^{-23}$	$1.17e^{-22}$	$1.19e^{-22}$	$1.18e^{-22}$	$1.19e^{-22}$						

 $\pi$ (C24-C25) distribute to  $\pi^*$ (C22-C23) and  $\pi$ (C26-C27)  $\to \pi^*$ (C24-C25) and  $\pi$ (C22-C23)  $\to \pi^*$ (C26-C27) and the delocalization from  $\pi$ (C6-C7)  $\to \pi^*$ (C2-C3) and  $\pi$ (C4-C5)  $\to \pi^*$ (C6-C7) and  $\pi$ (C4-C5)  $\to \pi^*$ (C2-C3) leading to some stabilization energy of 23.24, 21.61, 21.23 kcal/mol and 20.93, 20.81 and 19.95 kcal/mol as illustrated in Table (S2). The lone pair LP (2)-Se15 to antibonding  $\pi^*$ (C16-C21) having E(2) value 9.15 kcal/mol and  $\sigma$  electron delocalized from carbon and selenium (C13-Se15) to  $\sigma^*$  (O11-C12) represents less E(2) value of 7.97 kcal/mol was detected [36].

#### 4.9. Fukui function

The Fukui functions, which were computed from the NBO charges, define electrophilic and nucleophilic properties. It involves the computation of addition or termination of one electron from a molecule, it has a negative value when one electron is introduced to a molecule electron density is turn down. As a result, when density rose in some areas, the electron was removed from the molecule. [37] It demonstrates where density changes. The entire understanding of the reactivity order and position of electrophilic and nucleophilic sites is unmistakably explored by dual descriptors study. The atom C18 has large negative dual descriptive of −0.124 indicates that the atom has greater electroattack is in the order of C18>H43>H42>C27> H41>H40>C21>O29>C10>H48>H47>H37>C13>H31>H30 expressed in Table (S3). The highest positive dual descriptive for the atom C19 is 0.195, and it has a nucleophilic attack. In terms of reactivity, the atoms are in the following order C19>Se15>C20>C24> C17>H39>C16>C1>C8>C25>O11>C12>C7>H32>C3>H33>H45. [38]

Studying the local softness can provide insight into the significant role of biological investigations, as well as ligand and protein interactions.

# 4.10. NLO-properties

The simplest and least expensive method to discover the NLO characteristics is by DFT computing. The gas phase and other solvents (Acetone, ethanol, DMSO, water) of 3B6PL's properties were determined and tabulated in Table 4. Optoelectronics, optical data processing and numerous industrial applications all make use of nonlinear optical material. The NLO of Compounds is Resultant from polarizability of electrons in bonding orbitals [39]. The title compound has first order hyperpolarizability ( $\beta_0$ ), polarizability ( $\alpha$ ) and molecular dipole moment ( $\mu$ ) are  $5.8822 \times 10^{-30}$ esu,  $9.1721 \times 10^{-23}$  and 1.4584 Debye. In order to compare with urea which is the threshold material, it has the  $\beta_0$  value of  $(0.372 \times 10^{-30}$  esu). [40] As shown in Table (4)  $\beta_0$  of 3B6PL in gas phase is  $5.8822 \times 10^{-30}$ es.u., which is 16 folds more than urea. 25 times greater polarizability in acetone and ethanol ( $\beta_0 = 9.4634 \times 10^{-30}$ esu&  $9.4815 \times 10^{-30}$ esu) and 26 times greater in DMSO and water

 $(\beta_0{=}9.5131\times10^{-30} esu\&~9.5231\times10^{-30} esu).$  The differences in such properties support the solvents have made 3B6PL has more polarizable. Higher value of  $\beta_0$  and non-zero value of dipole moment results could indicate good NLO material, which are regarded as a crucial kinds of compound in medical chemistry.

#### 4.11. NMR studies

The magnetic properties of molecular nuclei are dependent on their chemical environment are a viable explanation for the geometrical, magnetic and chemical characteristics of 3B6PL using NMR. Utilizing TMS as an internal reference and DMSO-d<sub>6</sub> as solvent, the proton and carbon NMR of the 3B6PL was obtained as shown in Fig S1 (a) and (b). The combination of the NMR and computed simulation using GIAO technique yields a potent tool for deciphering and forecasting the structure of massive biomolecules. The 3B6PL was examined both experimentally and theoretically for <sup>1</sup>H NMR and <sup>13</sup>C NMR analysis, as shown in Table 5. In the  $\delta$ - lactone ring, the calculated chemical shift of  $^{13}\mathrm{C}$  NMR, C-atoms coupled with O and H-atom by double bonds were found to be 177.03 and 121.76 ppm for C10 and C13 atom, respectively. While 170.17 and 104.99 ppm were found to represent the comparable experimental shift. C28 is a methyl group, and it falls within the expected range of 10-40 ppm with a value of 21.83 ppm. [41] since the aromatic proton signals anticipated range is 4-9 ppm, the obtained theoretical chemical shift of H45, H35, H34, H41, and H33 which is from 7.6 to 7.45 ppm, is in accordance with the experimental results of 7.49 to 7.28 ppm. [42] Moreover, a quick scan of the literature revealed that the chemical shift measurements of related compounds showed very strong correlation.

Table 5 Observed and calculated  $^{13}$ C chemical shifts for 3B6PL in DMSO-d $_6$  solvent.

Atoms	Experimental (ppm)	Theoretical Chemical shift (ppm)
H45	7.491	7.6604
H35	7.471	7.6495
H34	7.381	7.5305
H41	7.361	7.5416
H33	7.284	7.4555
H37	2.924	3.0696
H48	2.685	2.7269
H9	2.509	2.7408
H30	2.491	2.7998
H38	2.418	2.5811
H50	2.377	2.3147
C10	170.17	177.031
C22	137.88	136.5981
C20	132.87	134.225
C19	130.35	131.5256
C13	104.99	121.7669
C1	41.5	41.2055
C14	35.33	38.8728
C28	21.41	21.8323

#### 4.12. Drug-likeness and ADME

# 4.12.1. Novel 3,5-dibenzyl-6-(p-tolyl)—3,4-dihydropyran-2-one exert drug-like properties

In order to identify drug-like properties resembling those found in medications, the Drug Determination Program (DDP) operates by evaluating a group and recognizing corresponding attributes.it does this by using physicochemical, lipophilicity, pharmacokinetics and drug likeness analyses. The online tool ADMET (Absorption, Distribution, Metabolism, Excretion, and Toxicity) can be employed for the purpose of scrutinizing these properties [43–46]. To evaluate the drug-like characteristics of our recently created molecule, we also used covert AI-based methods, such as study of Lipinski's rule of five and ADME, inside the same framework. According to Lipinski's rule, any chemical substance has to conform to a set of physicochemical characteristics in order to be considered suitable drug-like molecules.

The molecular weight should be (M.W. < 500 Da), the number of H-bond donors (HBDs: < 5) which is within range, H-bond acceptors (HBAs) must be less than 10, rotatable bonds should less than 10, to-pological polar surface area (TPSA) has the maximum thresholds of 140 Ų, and (Log P) remaining below the threshold of 5 constitute a number of these descriptors [26,27]. According to the initial drug-likeness study, the synthetic 3,5-dibenzyl-6-(p-tolyl)–3,4-dihydropyran-2-one met Lipinski's standards for acceptable scores of five as in Table 6. In brief, the synthesized compound was found to have a molecular weight (M.W.) of less than 500 daltons, and its HBD and HBA counts fell within the desired ranges of fewer than 5 and 10, respectively. On contrary, it was also demonstrated that the compounds have either 4 or 5 rotatable bonds, which is within the acceptable range of fewer than 10.

Contrarily, the permeability of drug candidate has frequently been evaluated using study of Log P in order to account for the possibility of hydrophobicity in the drug distribution pattern, while the TPSA is employed to determine the polarity and trans-membrane transit of substance [47]. Log P and TPSA analyses revealed the synthesized compound has an advantageous Log P value (Log P < 5). Additionally, the values for TPSA were reported as being less than 140 Ų for both manufactured and standard molecules (TPSA < 140 Ų, range 47.56 to 26.30 2), and less than 140 Ų for compounds. These characteristics show that the distinct synthesized molecule passes all drug-likeness tests which may then be evaluated potential pharmacological effects [48].

# 4.12.2. Novel 3,5-dibenzyl-6-(p-tolyl)—3,4-dihydropyran-2-one has acceptable ADME properties

The most important and essential point in the screening for chemical library for subsequent drug development is to predict various pharmacological metrics, such as ADME, utilizing AI-based in-silico techniques. The 3,5-dibenzyl-6-(p-tolyl)–3,4-dihydropyran-2-one that was synthesized showed variable aq. solubility ranging from 4599.46  $\rm mgL^{-1}$ , according to our ADME investigation. The anticancer drug of choice, bevacizumab, has the highest aq. solubility (642.480  $\rm mgL^{-1}$ ). However, blood-brain barrier (BBB) penetration scores (1.67161 C. brain/C. blood) were determined to be less than 2 [49–52]. To sum up, Table 7 reveals that the synthesized compound showed either poor or moderated transport against BBB.

The DDP's most important measurement has been identified as the assessment of the permeability of Caco-2 and MDCK cells [45–47]. PreADMET predicted the absorption of MDCK and Caco-2 cells. According to this investigation, the synthesized compound had a Caco-2 permeability range of 34.9837 nm/sec, which indicated that it had a moderate permeability toward Caco-2 cells. Similar to how the synthesized compound in the current investigation shown decreased permeability across MDCK cells, varied from 0.0444 for nm/sec. In several cellular models, the permeability scores of 4, Greater than 4 to 70 and Greater than 70 nm/sec indicate, respectively, low, intermediate, or elevated permeability [53].

An investigation of permeability through skin and epidermal linings, as well as the Caco-2, BBB and other MDCK cells are regarded to be of considerable significance as it deals with transdermal medicine delivery and unintentional contact with dangerous chemical compounds [54]. In this regard, it was found that the newly synthesized compound's skin permeability score (Log Kp) was negative (-2.4491 cm/h), which is within the permissible range for therapeutic medicines [55]. High M.W., solubility, and HBAs and HBDs are a few of the characteristics that control how medications behave after entering the bloodstream and reaching their intended target tissues, but plasma protein binding (PPB) may be the main unfavorable factor [56]. Chemical species with very high PPB scores typically exhibit greater circulating persistence or a longer plasma half-life (t1/2). More significantly, as the circulation percentage of drug is usually associated with their potent pharmacological actions, high PPB efficiency also affects therapeutic efficacy [57, 58]. The PPB for unique synthesized compound varied from 100 % to created chemical in a similar vein. Bevacizumab had a somewhat lower

Table 6
Drug-likeness studies of novel 3.5-dibenzyl-6-(p-tolyl)-3.4-dihydropyran-2-one

Molecular descriptors	Drug-likeness					
	MW (g/mol)	НВА	HBD	TPSA (Ų)	$Log K_p (cm/s)$	Rotatable bonds (RB)
Drug Bevacizumab	275.34	3	1	47.56	-6.41	4
Drug-like synthesized molecule	435.42	2	0	26.3	-4.71	5

**Table 7**ADME indices of novel 3,5-dibenzyl-6-(p-tolyl)—3,4-dihydropyran-2-one.

S. No.	Compounds	Skin permeability (logKp; cm/ h)	HIA (%)	BBB (C. Brain/C. Blood	Aq. Solubility (mg/L)	MDCK cell Permeability (nm/sec)	PPB (%)	CYT. p450 2D6 substrate	CYT. p450 2D6 inhibition	Caco2 cell permeability (nm/sec)
1	3,5-dibenzyl-6-(p- tolyl) – 3,4- dihydropyran-2-one	-2.4491	-1	1.67161	4599.46	0.0444	100	Non	inhibitor	34.9837
2	bevacizumab	-3.77187	95.0585	0.2162	642.48	187.974	70.9957	Non	inhibitor	53.7801

<sup>\*</sup>Human intestinal absorption (HIA): Blood brain barrier (BBB):Plasma protein binding (PPB).

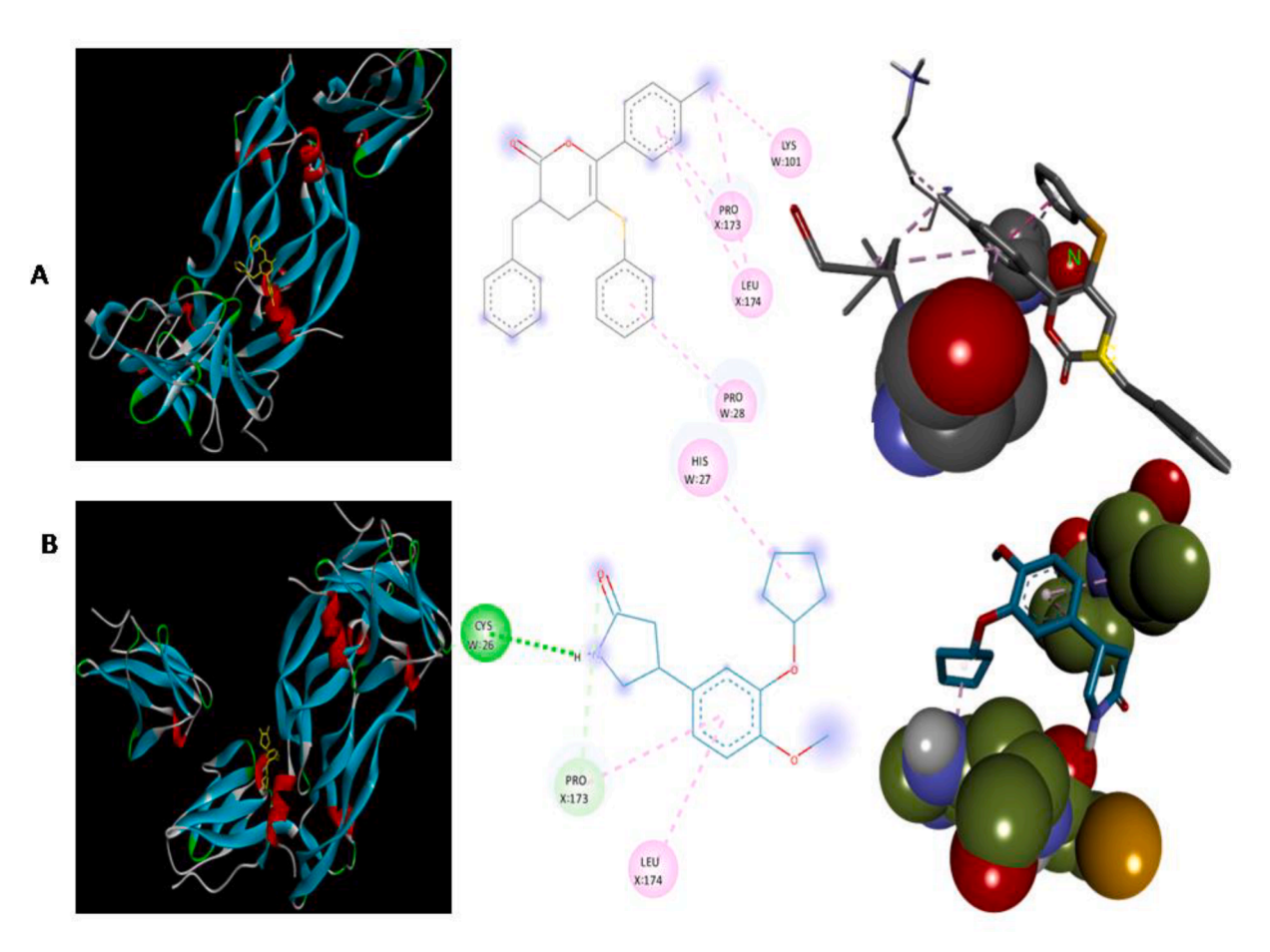


Fig. 9. Docked complexes with their 2D structures.

PPB efficiency (only 70.995 %), which may have been due to poor absorption and dispersion as well as its ineffectiveness in treating various cancers [59].

#### 4.13. Molecular docking studies

3,5-dibenzyl-6-(p-tolyl)-3,4-dihydropyran-2-one wasput through PvRx to find optimum inhibitor of the binding affinity domain of human 1QTY protein. The protein represented by a grid box of X=25xY=25 x Z = 25 points, and the grid spacing was employed X= 72.0897, Y = 48.5255, Z = 77.2097 [60]. Molecular docking holds significant value as a virtual technique for distinguishing stability of docked complexes considering their binding affinities (kcal/mol) at specific RMSD (root mean square deviation) values. Drug-like properties of selected synthesized compound have been successfully demonstrated. Further, we also evaluated their anticancer properties as a preliminary investigation using molecular docking. However, Bevacizumab has authorized by the FDA (Food and Drug Administration) as multipurpose drug to treat of cancer which was selected as a standard drug for the molecular docking investigations [61]. Actually, this drug is used in those types of cancer that develop endothelial cells related to the Flt-1 and kinase insert domain receptors of VEGFR. Although the VEGF receptor has greater significance not only in physiological but also in most pathological vasculogenesis as well as angiogenesis, like cancer, Therefore, docked complexes were showed the binding affinities -6.3 kcal/mol for the VEGFR-Ligand complex (A) and −5.9 kcal/mol of VEGFR-standard drug (B), respectively. Docked complexes with their 2D structures are shown in Fig. 9.

#### 5. Conclusions

In conclusion, we have successfully demonstrated the 3B6PL's potential inhibitor's impact against non-small cell lung, colorectal, renal, cervical, ovarian, fallopian tube, peritoneal, glioblastoma multiforme, and hepatocellular carcinomas as a preliminary test. Further, vibrational assignment was performed with PED, and the vibrations of 3B6PL were clearly seen in both theoretical and experimental spectra with high agreement. Theoretical geometrical parameters and experimental XRD results were examined and found to resonate. The experimental characterizations were accomplished for FT-IR, UV, XRD, and NMR. In UV-Vis spectra, molecules in various solvents exhibit identical absorption wavelengths that are in line with the results of experiments, demonstrating that the solvents are non-effective on the molecule's optical activity and that the electronic property is revealed. Moreover, HOMO-LUMO parameters indicate that 3B6PL was showed a good chemical reactivity; this molecule anticipated to have both positive and negative sites based on characteristic from MEP, surface analysis, and Fukui function. To gauge the level of electron localization, ELF was developed. The compound's structure has been resolved using NMR spectroscopy. Hirshfeld with dnorm, shapeindex, and curvedness with accompanying 2D fingerprint plots provides information on the intermolecular interaction and biological activity of the molecules. According to NBO research, the transition from anti-bonding  $\sigma^*(C10\text{-}O11)$  to lone pair (O29) transitions has the greatest influence and the highest stabilization energy. First order hyperpolarizability was used to explore the NLO characteristics, and the results demonstrate increased dipole moment, polarizability values in solvents phase, water and DMSO has 26 times higher polarizability than urea. The bioreactivity and toxic activity of the molecule were predicted by ADME and druglikeness, which

made it possible to use the molecule as a pharmaceutical compound. The docked complexes were demonstrating the binding affinities  $-6.3 \, \text{kcal/mol}$  for the VEGFR-Ligand complex (A) which is the lowest binding energy when compared to VEGFR- standard drug (B), this study shows the 3B6PL compound may have a greater anti-cancer activity.

#### CRediT authorship contribution statement

S. Durgadevi: Validation, Visualization, Writing – original draft, Writing – review & editing. C. Venkataraju: Formal analysis, Investigation. Malik Nasibullah: Data curation, Formal analysis, Software. Mohd Asif: Data curation, Formal analysis. Bhoopendra Tiwari: Investigation, Visualization, Resources. A. Manikandan: Conceptualization, Supervision, Data curation, Formal analysis, Funding acquisition, Investigation, Software. E. Geetha: Investigation, Methodology, Project administration, Software, Validation. S. Muthu: Formal analysis, Funding acquisition, Investigation, Visualization, Resources.

#### Declaration of competing interest

The authors declare that they have no known competing financial interests or personal relationships that could have appeared to influence the work reported in this paper.

#### Data availability

Data will be made available on request.

#### Research Data

All data are contained within the manuscript and supporting document.

## Supplementary materials

Supplementary material associated with this article can be found, in the online version, at doi:10.1016/j.chphi.2024.100482.

### References

- [1] I.A. Guedes, L.S.C. Costa, K.B. dos Santos, A.L.M. Karl, G.K. Rocha, I.M. Teixeira, M.M. Galheigo, V. Medeiros, E. Krempser, F.L. Custódio, H.J.C. Barbosa, M. F. Nicolás, L.E. Dardenne, Drug design and repurposing with DockThor-VS web server focusing on SARS-CoV-2 therapeutic targets and their non-synonym variants, Sci. Rep. 11 (2021) 1–20, https://doi.org/10.1038/s41598-021-84700-0.
- [2] O. Research, M. Asif, Fatmah FarrukhAqil, A. Alasmary, S.Almalki Amani, R. Khan Abdul, Malik Nasibullah, Lewis base-catalyzed synthesis of highly functionalized spirooxindole-pyranopyrazoles and their in vitro anticancer studies, Med. Chem. Res. 2023. (2023) 1–15, https://doi.org/10.1007/S00044-023-03053-7.
- [3] R.S. Verma, R. Talukdar, T. Azaz, B. Tiwari, Carbene catalyzed asymmetric synthesis of selenylated δ-lactones via [4+2] annulation of selenyl vinyl ketones and enals, Adv. Synth. Catal. (2022), https://doi.org/10.1002/ADSC.202201036.
- [4] A. Duenas-Gonzalez, Combinational therapies for the treatment of advanced cervical cancer, (2022). https://doi.org/10.1080/14656566.2022.2084689.
- [5] J. Summers, M.H. Cohen, P. Keegan, R. Pazdur, FDA drug approval summary: bevacizumab plus interferon for advanced renal cell carcinoma, Oncologist 15 (2010) 104, https://doi.org/10.1634/THEONCOLOGIST.2009-0250.
- [6] J.R. van Beijnum, E.J.M. Huijbers, K. van Loon, A. Blanas, P. Akbari, A. Roos, T. J. Wong, S.S. Denisov, T.M. Hackeng, C.R. Jimenez, P. Nowak-Sliwinska, A. W. Griffioen, Extracellular vimentin mimics VEGF and is a target for antiangiogenic immunotherapy, Nat. Commun. 131 (2022) 1–20, https://doi.org/10.1038/s41467-022-30063-7, 202213.
- [7] M.J. Frisch, G.W. Trucks, H.B. Schlegel, G.E. Scuseria, M.A. Robb, Gaussian 09, Revision E.01, Gaussian, Inc, Wallingford CT, 2009.
- [8] A.D. Becke, Density-functional thermochemistry, J. Chem. Phys. 98 (1993) 5648–5652.
- [9] Ksg. Dennington, Roy; Keith, Todd A.; Millam, John M. Semichem Inc., Shawnee Mission, Gaussview 06, 2016.
- [10] M.H. Jomroz, Vibrational Energy Distribution Analysis, VEDA4 (2004). Warsaw.
- [11] T. Lu, F. Chen, Multiwfn: a multifunctional wavefunction analyzer, J. Comput. Chem. 33 (2012) 580–592, https://doi.org/10.1002/jcc.22885.

- [12] M.A. Spackman, P.G. Byrom, A novel definition of a molecule in a crystal, Chem. Phys. Lett. 267 (1997) 215–220.
- [13] A. Daina, O. Michielin, V. Zoete, SwissADME: a free web tool to evaluate pharmacokinetics, drug-likeness and medicinal chemistry friendliness of small molecules, Sci. Rep 7 (2017) 42717, https://doi.org/10.1038/srep42717.
- [14] Dallakyan S., Olson A.J. Small-molecule library screening by docking with PyRx. Methods Mol Biol. 2015;1263:243–50.
- [15] N. Mills, ChemDraw Ultra 10.0", J. Am. Chem. Soc. 128 (41) (2006) 13649–13650, https://doi.org/10.1021/ja0697875.
- [16] Dassault Systemes BIOVIA: discovery studio visualizer 21.1.0.20298 (2020). 2021.
- [17] Origin, Origin 8.5. originlab corp, Northampton (2010)
- [18] A. Fatima, A. Ali, R. Rajan, I. Verma, S. Muthu, N. Siddiqui, P. Garg, S. Javed, Experimental spectroscopic, DFT, molecular docking, and molecular dynamics simulation investigations on m-phenylenediamine (Monomer and Trimer), Polycycl. Aromat. Compd (2022) 1–33, https://doi.org/10.1080/ 10406638.2022.2150655.
- [19] M. Medimagh, C.Ben Mleh, N. ISSAOUI, A.S. Kazachenko, T. Roisnel, O.M. Al-DOSSARY, H. Marouani, L.G Bousiakoug, DFT and molecular docking study of the effect of a green solvent (water and DMSO) on the structure, MEP, and FMOs of the 1-ethylpiperazine-1,4-diium bis(hydrogenoxalate) compound, J. Mol. Liq 369 (2023) 120851, https://doi.org/10.1016/j.molliq.2022.120851.
- [20] H. Abdelkader, Z. Farouk, M. Mohamed, M. Abdelghani, L. Houdheifa, K. Imene, H. Ines, B. Anis, C. Nadjib, H. Meriem, R. Souad, T. Lasnouni, L.B.. Omar, Efficient one-pot synthesis, characterization and DFT study of solvents polarity effects on the structural, energetic and thermodynamic proprieties of (a-methylamino-ethyl)-phosphonic acid dimethyl ester, J Mol. Struct 1272 (2023) 134165, https://doi.org/10.1016/j.molstruc.2022.134165.
- [21] M. Govindammal, M. Prasath, S. Kamaraj, S. Muthu, M. Selvapandiyan, Exploring the molecular structure, vibrational spectroscopic, quantum chemical calculation and molecular docking studies of curcumin: a potential PI3K/AKT uptake inhibitor, Heliyon 7 (2021) e06646, https://doi.org/10.1016/j.heliyon.2021.e06646.
- [22] A. FazilathBasha, F. Liakath Ali Khan, S. Muthu, M. Raja, Computational evaluation on molecular structure (Monomer, Dimer), RDG, ELF, electronic (HOMO-LUMO, MEP) properties, and spectroscopic profiling of 8-Quinolinesulfonamide with molecular docking studies, Computat. Theoretical Chem. 1198 (2021) 113169, https://doi.org/10.1016/j.comptc.2021.113169.
- [23] K.V. Prasad, M Sathish, A. Prabakaran, S.J. Basha, C. Santhamma, V. Vetrivelan, R. N. Devi, A. Irfan, S. Muthu, Vibrational energies, bonding nature, electronic properties, spectroscopic investigations and analysis of 3-bromo-4-Chlorobenzophenone, J. the Indian Chem. Soc. 99 (2022) 100735, https://doi.org/10.1016/j.jics.2022.100735.
- [24] A.A. Basha, F.L. Ali, S. Muthu, P. Mohamed, A. Kubaib, Dielectric relaxation, dipole moment, electronic characterization and non-covalent interaction behavior of valeramide and halo-phenol in non-polar liquid: a density functional theory-based approach, J Mol Liq 370 (2023) 121027, https://doi.org/10.1016/j. mollia.2022.121027.
- [25] N. Sheeja, G. Baskar, M. Thirunavukkarasu, S. Muthu, Covalent interaction, solvent effects, electrochemical, and spectroscopic characterization of novel (4Z)-4-{2-[amino(hydroxy)methyl]hydrazinylidene}-2,6-di(furan-2-yl)-3-methylpiperidin-1-ol derivative- anti-microbial activity study, J Mol Liq 374 (2023) 121272, https://doi.org/10.1016/j.molliq.2023.121272.
- [26] S. Sakthivel, T. Alagesan, S. Muthu, C.S. Abraham, E. Geetha, Quantum mechanical, spectroscopic study (FT-IR and FT - Raman), NBO analysis, HOMO-LUMO, first order hyperpolarizability and docking studies of a non-steroidal antiinflammatory compound, J Mol Struct 1156 (2018) 645–656, https://doi.org/ 10.1016/j.molstruc.2017.12.024.
- [27] C. Susan, S. Muthu, J. Christian, S. Armakovi, S.J. Armakovi, B.F. Rizwana, B. Geoffrey, H. Antony, R David, Computational evaluation of the reactivity and pharmaceutical potential of an organic amine: a DFT, molecular dynamics simulations and molecular docking approach, SpectrochimicaActa Part A 222 (2012) 117188. https://doi.org/10.1016/j.csa.2019.117188
- (2019) 117188, https://doi.org/10.1016/j.saa.2019.117188.
   [28] N. Agarwal, I. Verma, N. Siddiqui, S. Javed, Experimental spectroscopic and quantum computational analysis of pyridine-2,6-dicarboxalic acid with molecular docking studies, J Mol Struct 1245 (2021) 131046, https://doi.org/10.1016/j.molstruc.2021.131046.
- [29] S. Janani, H. Rajagopal, S. Muthu, S. Javed, A. Irfan, Structural, electronic properties (different solvents), chemical reactivity, ELF, LOL, spectroscopic insights, molecular docking and in vitro anticancer activity studies on methyl (4nitro-1-imidazolyl)acetate, J. Indian chem. Soc. 99 (2022) 100438, https://doi. org/10.1016/j.jics.2022.100438.
- [30] P. Sangeetha, S. Mullainathan, S. Muthu, A. Irfan, S. Sevvanthi, F.B. Asif, Electronic properties (in different solvents), spectroscopic progression and evaluation on 4morpholinepropane sulfonic acid along with molecular docking analysis, J Mol Liq 349 (2022) 118107, https://doi.org/10.1016/j.molliq.2021.118107.
- [31] V.S. Jeba Reeda, V. Bena Jothy, Mohd Asif, Malik Nasibullah, Naiyf S. Alharbi, Ghulam Abbas, S. Muthu, Synthesis, solvent polarity (polar and nonpolar), structural and electronic properties with diverse solvents and biological studies of (E) -3- ((3-chloro-4-fluorophenyl) imino) indolin-2-one, J Mol Liq 380 (2023) 121709, https://doi.org/10.1016/j.molliq.2023.121709.
- [32] S. Cherian Parakkal, R. Datta, A. Saral, S. Muthu, A. Irfan, A. Jeelani, Solvent polarity, structural and electronic properties with different solvents and biological studies of 3,3,5-triphenylfuran-2(3H)-one- cancers of the blood cells, J. Mol. Liq. 368 (2022) 120674, https://doi.org/10.1016/j.molliq.2022.120674.
- [33] G. Vijayakumari, N. Iyandurai, M. Raja, V. Vetrivelan, A. Thamarai, S. Saleem Javed, Muthu, Chemical reactivity, solvent effects, spectroscopic (FTIR, Raman, SERS, UV–Visible), hirshfeld analyses and antimalarial investigation of 3-

- Acetylbenzoic acid, Chem. Phys. Impact. 6 (2022) 100190, https://doi.org/10.1016/j.chphi.2023.100190.
- [34] S. Sarala, S.K. Geetha, S. Muthu, and F.B. Asif, Vibrational spectra and wavefunction investigation for antidepressant drug of amoxapine based on quantum computational studies, chemical data collections. 33(2021) 100699. htt ps://doi.org/10.1016/j.cdc.2021.100699.
- [35] S. Selvaraj, P. Rajkumar, M. Kesavan, S. Gunasekaran, S. Kumaresan, Experimental and theoretical analyzes on structural and spectroscopic properties of monomer and dimeric form of (S)-Piperidine-2-Carboxylic acid: an attempt on medicinal plant, Vib. Spectrosc. 100 (2019) 30–39, https://doi.org/10.1016/j. vibspec.2018.10.008.
- [36] A. Saral, R. Shahidha, M. Thirunavukkarasu, S. Muthu, Molecular structure, spectral, computational, IEFPCM investigation, and topological study on the biologically potent; cardiotonic drug 2-chloroquinolin-3-amine with structural optimization, Chem. Phys. Impact. 6 (2023) 100193, https://doi.org/10.1016/j.chpbi.2023.100193.
- [37] N. Siddiqui, S. Javed, Quantum computational, spectroscopic investigations on ampyra (4-aminopyridine) by dft/td-dft with different solvents and molecular docking studies, J. Mol. Struct. 1224 (2021) 129021, https://doi.org/10.1016/j molstruc.2020.129021
- [38] M. Vimala, S. Stella Mary, R. Ramalakshmi, S. Muthu, R. Niranjana Devi, A. Irfan, Quantum computational studies on optimization, donor-acceptor analysis and solvent effect on reactive sites, global descriptors, non-linear optical parameters of Methyl N-Boc-piperidine-3-carboxylate, J. Mol. Liq. 343 (2021) 117608, https:// doi.org/10.1016/j.molliq.2021.117608.
- [39] M. Vimala, S.S. Mary, R. Ramalakshmi, S. Muthu, Theoretical description of green solvents effect on electronic property and reactivity of Tert-butyl 4formylpiperidine-1-carboxylate, Comput. Theor. Chem. 1201 (2021) 113255, https://doi.org/10.1016/j.comptc.2021.113255.
- [40] A. Jeelani, S. Muthu, B. Narayana, Molecular structure determination, bioactivity score, spectroscopic and quantum computational studies on (E)-N<sup>-</sup>(4-Chlorobenzylidene)-2-(napthalen-2-yloxy) acetohydrazide, J. Mol. Struct. 1241 (2021) 130558, https://doi.org/10.1016/j.molstruc.2021.130558.
- [41] E. Eunice, Johanan Christian Prasana, S. Muthu, A. Anuradha, Molecular structure, spectroscopic, quantum computational, and molecular docking investigations on propyl gallate molecular structure, spectroscopic, quantum computational, Polycycl. Aromat. Compd (2022) 1–21, https://doi.org/10.1080/10406638.2022.2107688.
- [42] Khalid Karrouchi, Silvia A. Brandan, Yusuf Sert, Hakima El-marzouqi, Smaail Radi, Marilena Ferbinteanu, My El Abbes Faouzi, Yann Garcia, M'hammed Ansar, Synthesis, X-ray structure, vibrational spectroscopy, DFT, biological evaluation and molecular docking studies of (E)-N'-(4-(dimethylamino)benzylidene)-5-methyl-1Hpyrazole-3-carbohydrazide, J.Mol.Struct 1219 (2020), https://doi.org/10.1016/j. molstruc.2020.128541.
- [43] Gehad Lotfy, Yasmine M.Abdel Aziz, Mohamed M. Said, El Sayed H.El Ashry, El Sayed.H. ElTamany, MarwaM. AbuSerie, Mohamed Teleb, Alexander Dömling, Assem Barakat, Molecular hybridization design and synthesis of novel spirooxindole-based MDM2 inhibitors endowed with BCL2 signaling attenuation; a step towards the next generation p53 activators, Bioorg. Chem. 117 (2021) 105427. https://doi.org/10.1016/j.bioorg.2021.105427.
- [44] Hongbin Yang, Chaofeng Lou, Lixia Sun, Jie Li, Yingchun Cai, Zhuang Wang, Weihua Li, Guixia Liu, Yun Tang, AdmetSAR 2.0: web-service for prediction and optimization of chemical ADMET properties, Bioinformatics 35 (2019) 1067–1069, https://doi.org/10.1093/BIOINFORMATICS/BTY707.
- [45] P. Dhokne, A.P. Sakla, N. Shankaraiah, Structural insights of oxindole based kinase inhibitors as anticancer agents: recent advances, Eur. J. Med. Chem. 216 (2021) 113334, https://doi.org/10.1016/J.EJMECH.2021.113334.
- [46] Asif Mohd, Saquib Mohammad, Abdul Rahman Khan, AmanisalemAlmalki FarrukhAqil, Fatmah Ali Alasmary, Jaya Singh, Malik Nasibullah, Synthesis of Functionalized 2',5-Oxo-spiro[furan-2,3'-indoline]-3carboxylate Derivatives as Antiproliferative Agents: ADMET Studies, and

- Molecular Docking against P2Y12 Inhibitors, ChemistrySelect 8 (2023) e202204536, https://doi.org/10.1002/SLCT.202204536.
- [47] Y. Nahas, S. Prokhorenko, Q. Zhang, V. Govinden, N. Valanoor, L. Bellaiche, Topology and control of self-assembled domain patterns in low-dimensional ferroelectrics, Nat. Commun. 11 (2020) 1–8, https://doi.org/10.1038/s41467-020-19519-w
- [48] D. Galeano, S. Li, M. Gerstein, A. Paccanaro, Predicting the frequencies of drug side effects, Nat. Commun. 11 (2020) 1–14, https://doi.org/10.1038/s41467-020-18305-y.
- [49] C. Greene, N. Hanley, C. Reschke, A. Reddy, M. Mäe, R. Connolly, C. Behan, E. O'Keeffe, I. Bolger, N. Hudson, C. Delaney, M. Farrell, D. O'Brien, J. Cryan, F. Brett, A. Beausang, C. Betsholtz, D. Henshall, C. Doherty, M. Campbell, Microvascular stabilization via blood-brain barrier regulation prevents seizure activity, Nat Commun 13 (2022), https://doi.org/10.1038/s41467-022-29657-y
- [50] X.L. Ma, C. Chen, J. Yang, Predictive model of blood-brain barrier penetration of organic compounds, ActaPharmacol. Sin. 26 (2005) 500–512, https://doi.org/ 10.1111/j.1745-7254.2005.00068.x.
- [51] R. Leão, J. Cruz, G. da Costa, J. Cruz, E. Ferreira, R. Silva, L. de Lima, R. Borges, G. Dos Santos, C. Santos, Identification of new rofecoxib-based cyclooxygenase-2 inhibitors: a bioinformatics approach, Pharmaceuticals 13 (2020) 1–26, https://doi.org/10.3390/ph13090209.
- [52] Bailey Hiles-Murison, Andrew P. Lavender, Mark J. Hackett, Joshua J. Armstrong, Michael Nesbit, Samuel Rawlings, Terrence McGonigle, Andrew Warnock, Virginie Lam, John C.L. Mamo, Melinda Fitzgerald &RyuTakechi, blood-brain barrier disruption and ventricular enlargement are the earliest neuropathological changes in rats with repeated sub-concussive impacts over 2 weeks, Sci. Reports 11 (2021) 1–12, https://doi.org/10.1038/s41598-021-88854-9.
- [53] S. Yamashita, T. Furubayashi, M. Kataoka, T. Sakane, H. Sezaki, H. Tokuda, Optimized conditions for prediction of intestinal drug permeability using Caco-2 cells, Eur. J. Pharm. Sci. 10 (2000) 195–204, https://doi.org/10.1016/S0928-0987 (00)00076-2.
- [54] M. Lundborg, C.L. Wennberg, A. Narangifard, E. Lindahl, L. Norlén, Predicting drug permeability through skin using molecular dynamics simulation, J. Control. Release. 283 (2018) 269–279, https://doi.org/10.1016/j.jconrel.2018.05.026.
- [55] C.P. Chen, C.C. Chen, C.W. Huang, Y.C. Chang, Evaluating molecular properties involved in transport of small molecules in stratum corneum: a quantitative structure-activity relationship for skin permeability, Molecules 23 (2018) 911, https://doi.org/10.3390/molecules23040911.
- [56] S.S. Alvi, I.A. Ansari, M.K. Ahmad, J. Iqbal, M.S. Khan, Lycopene amends LPS induced oxidative stress and hypertriglyceridemia via modulating PCSK-9 expression and Apo-CIII mediated lipoprotein lipase activity, Biomed. Pharmacother. 96 (2017) 1082–1093, https://doi.org/10.1016/j.biopha.2017.11.116.
- [57] J.A. Roberts, F. Pea, J. Lipman, The clinical relevance of plasma protein binding changes, Clin Pharmacokinet 52 (2013) 1–8, https://doi.org/10.1007/s40262-012.0018.5
- [58] K.G. Gurevich, Effect of blood protein concentrations on drug-dosing regimes: practical guidance, Theor. Biol. Med. Model 10 (2013) 20, https://doi.org/ 10.1186/1742-4682-10-20
- [59] J. Kim, H. Cho, J. Kim, C. Shim, S. Chung, M. Oak, I. Yoon, D. Kim, The limited intestinal absorption via paracellular pathway is responsible for the low oral bioavailability of doxorubicin, Xenobiotica 43 (2013) 579–591, https://doi.org/ 10.3109/00498254.2012.751140
- [60] S. Bharadwaj, A. Dubey, N.K. Kamboj, A.K. Sahoo, S.G. Kang, U. Yadava, Drug repurposing for ligand-induced rearrangement of Sirt2 active site-based inhibitors via molecular modeling and quantum mechanics calculations, Sci. Rep. 11 (2021) 10169, https://doi.org/10.1038/s41598-021-89627-0.
- 10169, https://doi.org/10.1038/s41598-021-89627-0.
  [61] K. Vedhapriya, G. Balaji, B. Dhiyaneshwari, Ahmad Irfan, M. Thirunavukkarasu, S. Kaleeswaran, Safia Obairdur Rab, S. Muhtu, Effect of green solvents, molecular structure and topological studies on 4-amino-1-β-D-ribofuranosyl-1,3,5 triazin-2 (1H)-one anti-blood cancer agent, J. Indian Chem. Soc. (2023) 100912, https://doi.org/10.1016/j.jics.2023.100912.